Converter-level reliability of wind turbine with low sample rate mission profile

Zhou, Dao; Blaabjerg, Frede

Published in:
Proceedings of 2019 10th International Conference on Power Electronics and ECCE Asia (ICPE 2019 - ECCE Asia)

Publication date:
2019

Document Version
Accepted author manuscript, peer reviewed version

Converter-level Reliability of Wind Turbine with Low Sample Rate Mission Profile

Dao Zhou, and Frede Blaabjerg

Department of Energy Technology
Aalborg University, Aalborg, Denmark
zda@et.aau.dk; fbl@et.aau.dk

***Abstract* - The thermal dynamics of power semiconductors and power capacitors are closely related to the reliability and the cost of power electronic converter. However, the component loading in a wind turbine system is disturbed by many factors of the converter system, which is present at various time-constants from micro-seconds to years. In the case of a mission profile with 1-hour sample rate, the circuit model, loss model, and thermal model of the active power switches and passive capacitors are described and presented. The percentile lifetime of a single component can be predicted according to the long-term electro-thermal profile, and the Weibull function based time-to-failure distribution of the active component and passive component can be obtained. In a 2 MW wind turbine system, it can be seen that the dc-link capacitor bank dominates the converter-level reliability.**

I. INTRODUCTION

Power electronics are being widely used in many energy conversion systems like renewable energy, motor drives, transportation and power transmission. The reliability and cost requirements for these power electronic systems are getting more critical [1]-[7]. For the reliability-critical components (e.g. power semiconductor and power capacitor), their thermal loading are especially important. It has been found that the dynamic changes of thermal stress is one of the most critical causes of wear-out failure. Consequently, a correct modeling for the thermal behavior is a crucial step to evaluate the reliability performance.

A typical wind power system is illustrated in Fig. 1, and the main disturbances for the thermal behavior of the power semiconductor and capacitor are summarized according to their dominant response time. It is noted that these thermal disturbances have very different time constants ranging from microseconds (device switching, capacitor ripple current) to hours (ambient temperature changing), making the sampling step of the models in the converter system hard to be decided. The existing models for power electronics seem not good enough to reflect the thermal performance: either very detailed circuit models are applied but restrained to limited timespan and small time-step [8], or only steady-state conditions are assumed with a compromised accuracy of many of the important thermal dynamics [9].

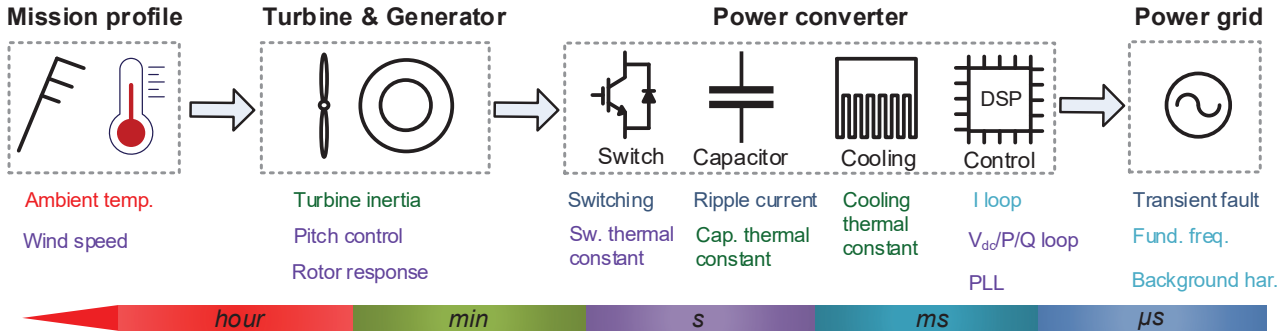

Fig. 1. Timescale in wind turbine system.

II. RELIABILITY ISSUE IN ACTIVE COMPONENTS

A typical configuration of a Doubly-Fed Induction Generator (DFIG) is graphically shown in Fig. 2. The partial-scale power converter consists of the Rotor-Side converter (RSC) and the Grid-Side Converter (GSC), due to their positions. In between, a dc-link capacitor bank is applied to decouple the back-to-back power converter. Besides, an LCL filter is employed in order to eliminate the high-order harmonics caused by the PWM modulation. As investigated in [2], the power switches and capacitor banks are among the top three fragile components in the power electronic converter, so it is important to evaluate their reliability issues.

As shown in Fig. 3(a), an annual wind speed (Class I) and ambient temperature are sampled every hour. Since the sample

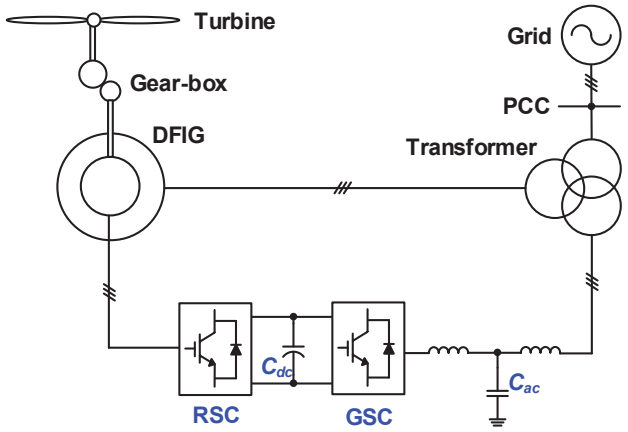

Fig. 2. Typical configuration of a doubly-fed induction generator system. The partial scale power converter consists of the RSC (rotor-side converter) and the GSC (grid-side converter).

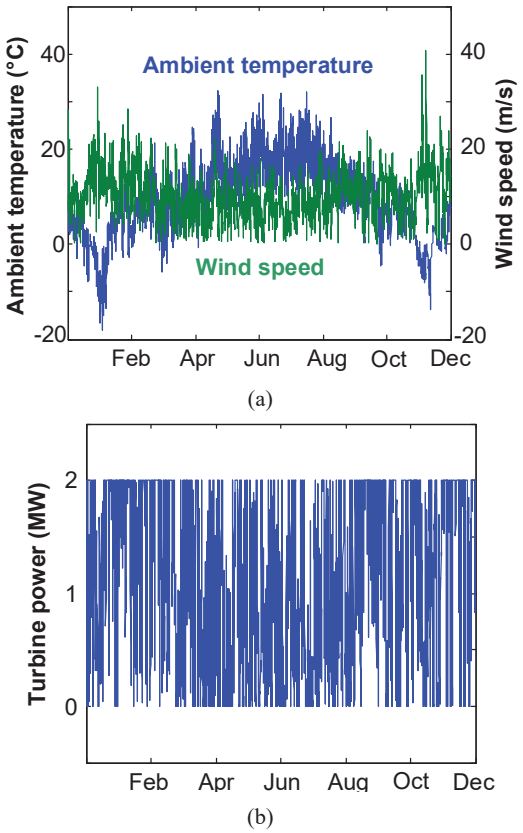

Fig. 3. Mission profile of a 2 MW wind turbine with sample rate of 1 hour. (a) Wind speed and ambient temperature. (b) Turbine output power.

rate is low enough to neglect the dynamics in the turbine and generator, the turbine output power is illustrated in Fig. 3(b). It is worthwhile to note that the cut-in wind speed is 4 m/s, the rated wind speed is 12 m/s, and the cut-off wind speed is 25 m/s.

TABLE I
PARAMETERS OF 2 MW DFIG SYSTEMS

Rated power	2 MW
Operational range of rotor speed	1050-1800 rpm
Rated amplitude of phase voltage	563 V
Mutual inductance	2.91 mH
Stator leakage inductance	0.04 mH
Rotor leakage inductance	0.06 mH
Ratio of stator winding and rotor winding	0.369
DC-link voltage	1050 V
DC-link capacitor	20 mF
Grid-side inductor	125 μH
Converter-side inductor	125 μH
AC-side filter capacitor	300 μF
Switching frequency	2 kHz

TABLE II
PARAMETERS USED IN LOSS MODEL AND THERMAL MODEL OF POWER SEMICONDUCTORS

		IGBT	Diode
Loss model	V_{ce} @ 1 kA, T_j=150 ºC (V)	2.45	/
	V_f @ 1 kA, T_j=150 ºC (V)	/	1.95
	E_{on} @ 1 kA, T_j=150 ºC (mJ)	430	/
	E_{off} @ 1 kA, T_j=150 ºC (mJ)	330	/
	E_{rr} @ 1 kA, T_j=150 ºC (mJ)	/	245
Thermal model	Fourth order thermal resistance R (ºC/kW)	0.3	0.48
		1.6	3.61
		18	34.6
		3.1	6.47
	Fourth order thermal time constant τ (s)	0.003	0.0002
		0.0013	0.0009
		0.04	0.03
		0.4	0.2

As the rotor-side active power is the product of the stator-side power and the generator slip, together with the relationship between the slip and wind speed, the power flowing through the back-to-back power converters can be obtained by [10]. The flowchart to estimate the lifetime of the power switches is shown in Fig. 4. With the help of the generator and converter circuit models, the converter voltage and current can be calculated. On the basis of the conduction loss and switching loss, the loss dissipation of the IGBT and the freewheeling diode can be found. By using the thermal model, which only takes into account the thermal resistance of power device and cooling method (due to the 1-hour sample rate), the junction temperature of the IGBT and the diode can be deduced. As the annual thermal profile is irregular, the Rainflow counting is then applied to extract the thermal cycles with their corresponding amplitude, mean value, and period.

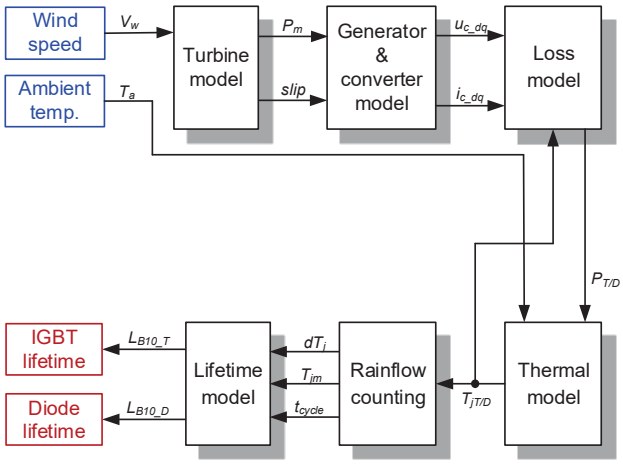

Fig. 4. Flow-chart to calculate B_{10} lifetime of the power switches from mission profile.

The B_{10} lifetime of the IGBT and the diode can be calculated according to the Coffin-Manson lifetime model [11].

A case study is conducted in a 2 MW DFIG system, whose specification is listed in Table I. The annual operating profiles of the IGBT and the diode in the GSC are shown in Fig. 5. The key loss and thermal parameters of the power semiconductors are summarized in Table II. As the majority of the power flows from the dc-link to the power grid, it is evident that the IGBT loss is much higher than the diode loss. Nevertheless, the diode chip size is typically almost a half of the IGBT chip, so the junction temperature of the IGBT is just a little higher than the diode. Eventually, it can be seen that the annual damage of the IGBT is 1.2% compared to the diode of 0.9%. Due to the sample rate of 1 hour, it is worthwhile to mention that the thermal cycles are with a period higher than 1 hour after the Rainflow counting algorithm. In addition, only the power switches in the GSC is considered.

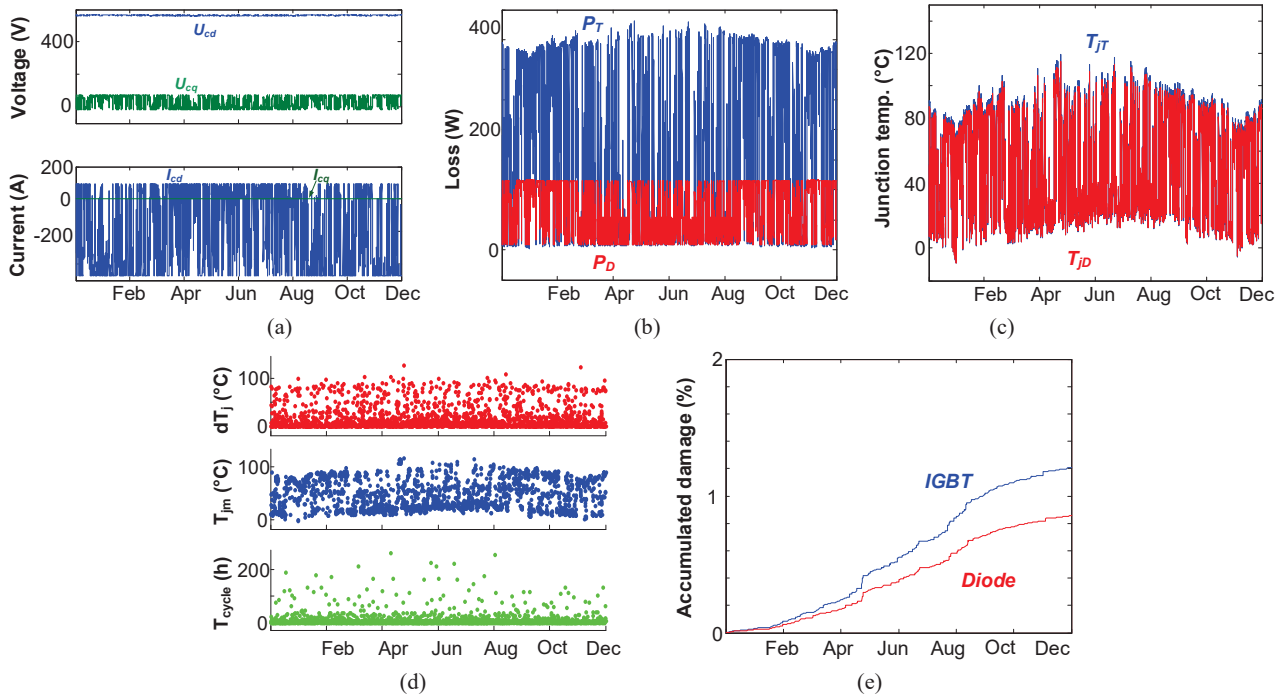

Fig. 5. Annual profile of the IGBT and the diode in the grid-side converter. (a) Electrical stresses. (b) Loss profiles. (c) Thermal profiles. (d) Rainflow counting results. (e) Annual damage.

III. Reliability Issue in Passive Components

In this section, an analytical approach to assess the reliability for power capacitors, both the DC-link capacitor bank (Al-CAP) and AC-side filter capacitor bank (MPF-CAP), is presented considering the annual mission profile. Based on the electrical behavior at various loading conditions, the lifecycle of the single power capacitor can be predicted through its electro-thermal stresses.

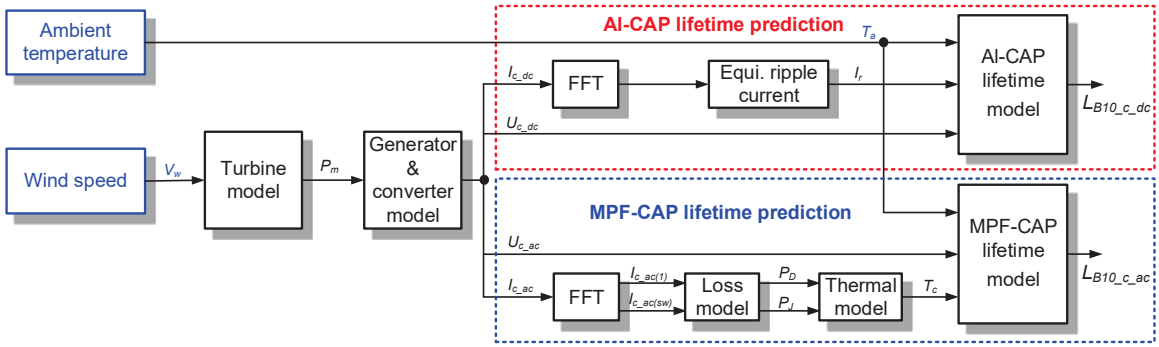

Fig. 6. Flow-chart to calculate B_{10} lifetime of ac-side and dc-link capacitors.

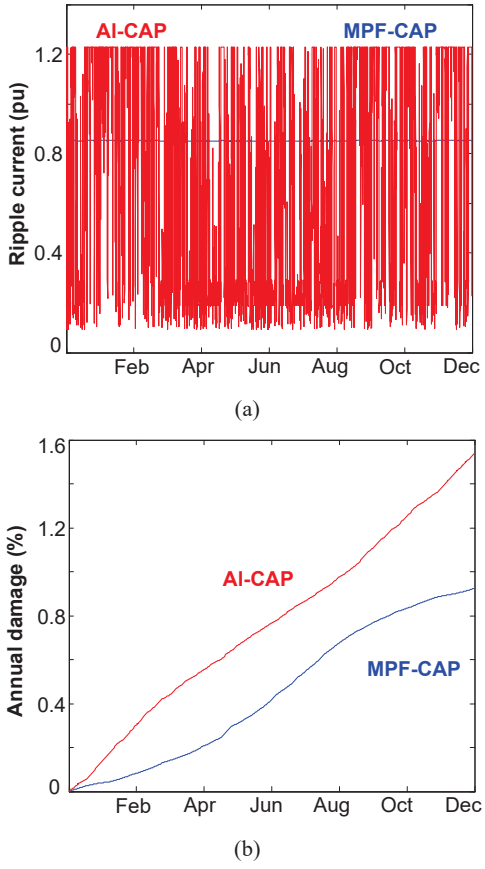

Fig. 7. Annual damage profile comparison between the metalized polypropylene film capacitor (MPF-CAP) and the aluminum electrolytic capacitor (Al-CAP). (a) Ripple current. (b) Accumulated damage.

According to the mission profile of the wind turbine system, the general procedure to calculate the lifetime of the Al-CAP and MPF-CAP is shown in Fig. 6 [12]. In respect to the Al-CAP, the ripple current can be calculated with the PWM pattern of power switches in the back-to-back power converters. It is worth mentioning that, considering the ESR curve with the various frequencies, the dominating switching harmonics need to be converted to 100 Hz, which is normally specified in the DC-link capacitor datasheet. Together with the ambient temperature profile, the life expectancy of the Al-CAP can be predicted [12].

TABLE III

PARAMETERS OF CAPACITORS THERMAL AND LIFETIME MODELS

	Al-CAP	MPF-CAP
Rated lifetime L_r (hour)	6,000	100,000
Upper categorized temperature T_r (ºC)	105	75
Rated ripple current I_r (A)	13.4	30
Rated voltage V_r (V)	400	780
Core temperature rise at rated ripple current ΔT_o (ºC)	10	/
Coefficient of temperature rise n_1	5	/
Voltage exponent coefficient n_2	5	0.7
ESR (mΩ)	/	3.0
Dissipation factor tanδ	/	2e-4
Thermal resistance from core to ambient (ºC/W)	/	14.1

As the lifetime model of the MPF-CAP is tightly related to its core temperature and the applied voltage, the procedure slightly differs with the Al-CAP. Considering both the dielectric loss and the Joule loss dissipation, the core temperature of the capacitor can be jointly decided by the core-ambient thermal resistance and the ambient temperature profile. With the applied voltage calculated by the PWM pattern of the power switch and the characteristics of the LCL filter, the lifetime of the MPF-CAP can be estimated.

As the sample time interval is much higher than the capacitor thermal time constant (typically several minutes), it can roughly be assumed that the core temperature of the capacitor reaches steady-state and stays constant within every sample period. The lifetime damage can thereby be calculated by using the sample period over its corresponding hours to failure, which is accumulated from a sample period to the whole operational year.

Based on the key parameters related to the capacitor lifetime prediction listed in Table III, the annual damage of the both types of the capacitors can be deduced and it is shown in Fig. 7, where the lifecycle of the capacitor runs out when the

accumulated damage reaches 1. It is worthwhile to mention that the hours to failure is defined as the B10 lifetime. It can be seen that the ripple current of the MPF-CAP is much smoother, as the current harmonic hardly changes with different wind speeds. Moreover, the annual damage of the MPF-CAP is lower, due to the fact that it contains much longer rated lifetime (100,000 hour) compared to the Al-CAP (6,000 hour) under the rated operating condition.

IV. Time-to-Failure and Reliability of Filter Capacitor Bank

In this section, the percentile lifetime of the single active and passive component will be translated to the Weibull lifetime distribution. Therefore, the converter-level reliability can be linked from the component-level reliability by using the reliability block diagram.

In order to fulfill the high enough capacitance or withstand the voltage stress, plenty of the capacitors are connected in series or parallel in order to form the capacitor bank. Since any failure of the individual capacitor may result in a degraded performance of the capacitor bank, and any failure of the IGBT or the diode induces the improper operation of the two-level power converter, all of the power switches and capacitors are connected in series in the reliability block diagram as shown in Fig. 8.

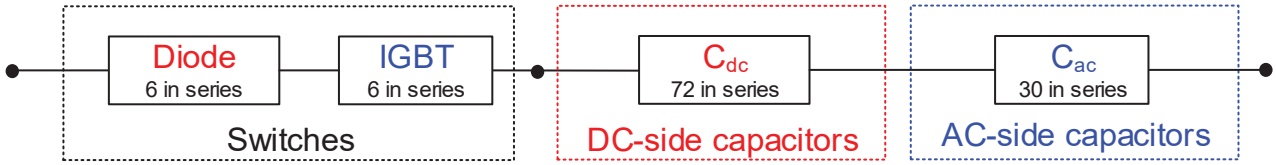

Fig. 8. Converter-level reliability block diagram consisting of the power switches, dc-side capacitors ,and ac-side capacitors.

Based on the annual damage of both the active and passive components shown in Fig. 5(e) and Fig. 7(b), their B_{10} lifetime can be deduced. In order to assess the converter-level reliability performance, the B_{10} lifetime of the individual component is insufficient, and its time-to-failure distribution, which considers the parameter variations and tolerance uncertainties, is required in order to apply the reliability block calculation. Since the Weibull shape parameters of the power switches and power capacitors are provided in [6], [7], their unreliability curve along with the operational hour can be obtained as shown in Fig. 9(a) and (b). For the power switches, as the power converter contains six IGBTs and six diodes, at the desired 20-year B_{10} lifetime of the wind power converter, the unreliability value of the total switches significantly increases to 1.2%, while the unreliability value of the individual IGBT is lower than 0.2%. For the power capacitors, it can be seen that the unreliability value of the dc-link capacitor bank and the ac-side filter capacitor bank becomes 1.8% and 0.1% at the desired lifespan. The converter-level unreliability is shown in Fig. 10(c), it is noted that the capacitor bank dominates the converter-level lifetime. Furthermore, the unreliability value at the desired lifespan is 3.1%, which fulfills the 20-year designed lifecycle.

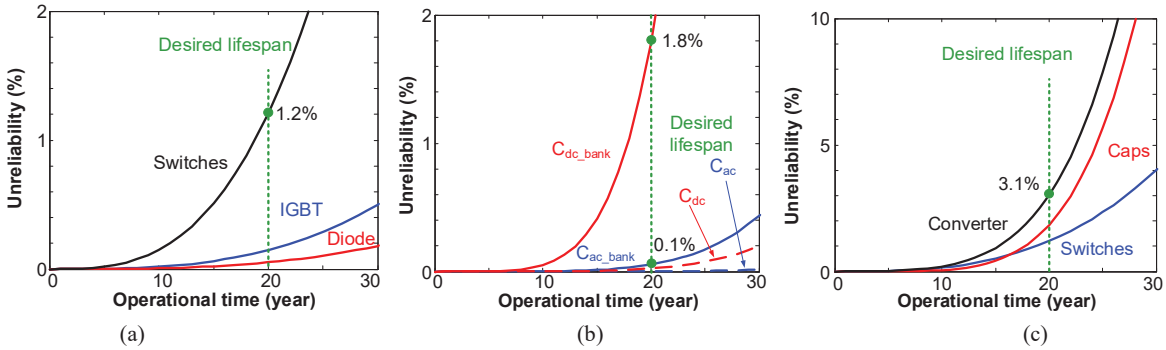

Fig. 9. Unreliability curve from the single component to power converter. (a) From IGBT and diode to power switches. (b) From single capacitor to capacitor bank. (c) From switches and capacitors to power converter.

V. Conclusion

In this paper, the interested timescales of the wind turbine system are mapped in terms of the mechanical and electrical parts. In the case of the mission profile with 1-hour sample rate, the circuit model, loss model, and thermal model of the active power switches and passive power capacitors can be considerably simplified. The percentile lifetime of single component can be predicted according to the long-term electro-thermal profile. By considering the parameter variations and component tolerance, the Weibull function based time-to-failure distribution of the active component and passive component can be obtained. In a 2 MW doubly-fed induction generator based wind turbine system, it can be seen that the dc-link capacitor bank dominates the converter-level reliability. However, to obtain an accurate comparison, the

mission profile with higher resolution can be suggested to take the thermal cycling lower than 1-hour into account.

References

[1] F. Blaabjerg, and K. Ma, "Future on power electronics for wind turbine systems," *IEEE Journal of Emerging and Selected Topics in Power Electronics*, vol. 1, no. 3, pp. 139-152, Sept. 2013.

[2] H. Wang, M. Liserre, F. Blaabjerg, P. Rimmen, J. Jacobsen, T. Kvisgaard, and J. Landkildehus, "Transitioning to physics-of-failure as a reliability driver in power electronics," *IEEE Journal of Emerging and Selected Topics in Power Electronics,* vol. 2, no. 1, pp. 97-114, Mar. 2014.

[3] M. Liserre, R. Cardenas, M. Molinas, and J. Rodriguez, "Overview of multi-MW wind turbines and wind parks," *IEEE Trans. on Industrial Electronics*, vol. 58, no. 4, pp. 1081-1095, Apr. 2011.

[4] V. de N. Ferreira, A. F. Cupertino, H. A. Pereira, A. V. Rocha, S. I. Seleme, and B. de J. C. Filho, "Design and selection of high reliability converters for mission critical industrial applications: a rolling mill case study," *IEEE Trans. on Industry Applications*, vol. 54, no. 5, pp. 4938-4947, Sep. 2018.

[5] F. Richardeau, and T. T. L. Pham, "Reliability calculation of multilevel converters: theory and applications," *IEEE Trans. on Industrial Electronics*, vol. 60, no. 10, pp. 4225-4233, Oct. 2013.

[6] Z. Zhao, K. Li, Y. Jiang, S. Lu, and L. Yuan, "Overview on reliability of modular multilevel cascade converters," *Chinese Journal of Electrical Engineering*, vol. 1, no. 1, pp. 37-49, Dec. 2015.

[7] J. Kiilunen, and L. Frisk, "Reliability analysis of two frequency converter generations using system-level stress testing," *IET Power Electronics*, vol. 5, no. 7, pp. 1042-1048, Aug. 2012.

[8] D. Zhou, F. Blaabjerg, M. Lau, and M. Tonnes, "Optimized reactive power flow of DFIG power converters for better reliability performance considering grid codes," *IEEE Trans. on Industrial Electronics*, vol. 62, no. 3, pp. 1552-1562, Mar. 2015.

[9] K. Ma, M. Liserre, F. Blaabjerg, and T. Kerekes, "Thermal loading and lifetime estimation for power device considering mission profiles in wind power converter," *IEEE Trans. on Power Electronics*, vol. 30, no. 2, pp. 590-602, Feb. 2015.

[10] D. Zhou, G. Zhang, and F. Blaabjerg, "Optimal selection of power converter in DFIG wind turbine with enhanced system-level reliability," *IEEE Tran. on Industry Applications*, vol. 54, no. 4, pp. 3637-3644, Jul. 2018.

[11] P. Lall, M. N. Islam, M. K. Rahim, and J. C. Suhling, "Prognostics and health management of electronic packaging," *IEEE Trans. on Components and Packaging Technologies*, vol. 29, no. 3, pp. 666-677, Sep. 2006.

[12] D. Zhou, Y. Song, Y. Liu, and F. Blaabjerg, "Mission profile based reliability evaluation of capacitor banks in wind power converters," *IEEE Trans. on Power Electronics*, vol. 34, no. 5, pp. 4665-4677, May 2019.